

# Wholly vascularized millimeter-sized engineered tissues by cell-sized microscaffolds



Y. Naka<sup>a</sup>, S. Kitano<sup>b</sup>, S. Irie<sup>b</sup>, M. Matsusaki<sup>a,b,\*</sup>

<sup>a</sup> Department of Applied Chemistry, Graduate School of Engineering, Osaka University, 2-1 Yamadaoka, Suita, Osaka, 565-0871, Japan

<sup>b</sup> Joint Research Laboratory (TOPPAN) for Advanced Cell Regulatory Chemistry, Graduate School of Engineering, Osaka University, 2-1 Yamadaoka, Suita, Osaka, 565-0871, Japan

## ARTICLE INFO

### Keywords:

Tissue engineering  
Extracellular matrix  
Micrometer-sized scaffold  
Collagen microfiber  
Vascularization

## ABSTRACT

The *in vitro* fabrication of wholly vascularized millimeter-sized engineered tissues is still a key challenge in the tissue engineering field. Recently we reported a unique approach ‘sedimentary culture’ using a collagen microfiber (CMF) to fabricate large-scale engineered tissues. The millimeter-sized tissues with high extracellular matrix (ECM) density were easily obtained by centrifugation of cells and CMFs and subsequent cultivation because the CMFs acted as a micrometer-sized scaffold. However, cell distribution in the obtained tissues was not homogeneous because of the different sedimentation velocity of the cells and CMFs because of their size difference.

Here we report the fabrication of wholly vascularized millimeter-sized engineered tissues using cell-sized CMFs. To avoid dissolving, vacuum drying was performed at 200 °C for 24 h for thermal crosslinking of primary amine groups of type I collagen. The 200- and 20- $\mu\text{m}$ -sized CMFs (CMF-200 and CMF-20) were obtained by homogenization and subsequent sonication of the crosslinked collagen. Interestingly, the CMF-20 indicated a similar sedimentation velocity with cells because of their same size range, thus uniform millimeter-sized tissue with homogeneous cell distribution was fabricated by the sedimentary culture method. To form a whole blood capillary structure in the tissues, fibronectin (FN) was adsorbed on the surface of CMF-20 to stimulate endothelial cell migration. The distribution of the blood capillary network in 1.6-mm-sized tissues was markedly improved by FN-adsorbed CMF-20 (FN-CMF-20). Sedimentary culture using FN-CMF-20 will create new opportunities in tissue engineering for the *in vitro* fabrication of wholly vascularized millimeter-sized engineered tissues.

## 1. Introduction

A current key challenge in tissue engineering is *in vitro* vascularization of large-scale engineered tissues with greater than millimeter size that can be used for clinically relevant therapies and as a drug-testing model. Blood capillaries, which are composed of an endothelial monolayer, pericytes (or smooth muscle cells), and fibroblasts, maintain the metabolic activities and functions of organs through the transportation of nutrients and oxygen [1]. The introduction of these vasculatures into engineered tissues has the advantages of avoiding necrosis of the inner cells and of enhancing the cell functions in the tissues through cellular signaling [2,3]. To develop the vascularized tissues, many attempts such as a three-dimensional (3D) culture of endothelial cells in hydrogels composed of extracellular matrix (ECM) [4,5], the fixation of angiogenic factors into scaffolds [6–11], cell sheet engineering for transplantable tissues [12–14], ECM nanocoating on cell surfaces [15–17], and

microfluidics [16–18] have been reported. Although these are effective methods of constructing vascularized tissues, there is a size limitation for whole vascularization in millimeter-scale tissues.

There are generally two approaches, top-down and bottom-up in tissue engineering for the *in vitro* fabrication of 3D-engineered tissues [19]. The top-down approach uses a porous scaffold composed of materials such as sponges, hydrogels, or fibers, and thus homogeneous cell migration from the surface to the interior is necessary to obtain uniform tissues. It is therefore difficult to obtain high cell distribution in the millimeter-sized scaffolds due to limitation of cell migration (cell size is ca. 15  $\mu\text{m}$ ). Recently, perfusion culture of adipose-derived stromal vascular fraction cells in collagen scaffolds has been reported to promote *in vitro* the early formation of a capillary-like network [20]. Although it was difficult to fabricate wholly vascularized tissues *in vitro*, the pre-vascularization accelerated *in vivo* vascularization of the engineered tissues. In the bottom-up approach, scaffold-free method provides cell

\* Corresponding author. Department of Applied Chemistry, Graduate School of Engineering, Osaka University, 2-1 Yamadaoka, Suita, Osaka, 565-0871, Japan.  
E-mail address: [m-matsus@chem.eng.osaka-u.ac.jp](mailto:m-matsus@chem.eng.osaka-u.ac.jp) (M. Matsusaki).

<https://doi.org/10.1016/j.mtbio.2020.100054>

Received 5 March 2020; Received in revised form 11 April 2020; Accepted 11 April 2020

Available online 28 April 2020

2590-0064/© 2020 The Author(s). Published by Elsevier Ltd. This is an open access article under the CC BY-NC-ND license (<http://creativecommons.org/licenses/by-nc-nd/4.0/>).

aggregations or multilayers with high cell density, and the scaling up of such high cell density tissues to over 200  $\mu\text{m}$  is difficult because of the diffusion issue of nutrient and oxygen. For these well-documented reasons, the fabrication of wholly vascularized engineered tissues with homogeneous cell distribution is still a challenge.

In our body, blood capillaries are embedded in connective tissue whose main component is ECM, especially type I collagen [21,22]. It is therefore important to construct 3D tissues with a high collagen concentration rather than high cell density for blood capillary formation. The classic collagen gels have been in use for several decades and improvements are thus needed, concerning their relevance with respect to *in vivo* similarity, for applications in tissue engineering and regenerative medicine. However, classic collagen gels can only show a maximum collagen dilution of 0.3%, far from the 25–35% present in connective tissue [23]. Although fibroblasts cultured in the scaffolds can secrete collagen by themselves, it takes long time to obtain such high collagen density. This differs considerably from that present in living tissue, where a large, dense, and well-organized network of collagen type I fibers appears around the cells. To simulate this extracellular microenvironment, the use of collagen in the form of fibers instead of gels can be the physiological solution from a biophysical perspective, allowing forces and energy transmission, or providing biological signals to adjacent cells and regulating functional responses [24].

We recently reported a unique tissue engineering technique ‘sedimentary culture’ using collagen microfibers (CMFs) leading to a large-scale engineered tissue with high collagen density (up to 20–30 wt%), similar to *in vivo* connective tissues [25–27]. The millimeter-sized engineered tissues with high collagen density were easily obtained by centrifugation and subsequent cultivation because the CMF acted as a micrometer-sized scaffold. The secreted ECM from the cultured fibroblasts acted as a crosslinker to assemble CMF and the cells as a uniform tissue. Although this is a simple and powerful method of obtaining large-scale tissues consisting of cells and ECMs within 1 week, cell distribution in the resultant tissues was not homogeneous because of the different sedimentation velocity of the cells and CMF because of the size difference between the 15  $\mu\text{m}$  diameter cells and the 200  $\mu\text{m}$  length CMF. To successfully produce millimeter-sized engineered tissues with high ECM density and uniform blood

capillaries, down-sizing of CMF to cell size range would be necessary to optimize sedimentation velocity.

Here we report the fabrication of wholly vascularized millimeter-sized engineered tissues using cell-sized CMFs (Fig. 1). To avoid water dissolving, vacuum drying was performed for thermal crosslinking of type I collagen sponge. The 20- $\mu\text{m}$ -sized CMF (CMF-20) was obtained by homogenization and subsequent sonication of the crosslinked collagen. Interestingly, uniform millimeter-sized tissues with high cell distribution were fabricated by sedimentary culture because of the similarity of sedimentation velocity of CMF-20 with normal human dermal fibroblasts (NHDFs). To form a whole blood capillary structure in the tissues, fibronectin (FN) was adsorbed on the surface of CMF-20 to improve endothelial cell migration. The homogeneous distribution of blood capillary networks in 1.6-mm-sized tissues using FN-adsorbed CMF-20 (FN-CMF-20) was clearly observed using confocal laser scanning microscopy (CLSM). The sedimentary culture using FN-CMF-20 will be a fundamental technology for the fabrication of wholly vascularized millimeter-sized tissues in the tissue engineering field.

## 2. Materials and methods

### 2.1. Materials

Porcine type I collagen sponge was kindly donated by Nippon Ham Foods Ltd. (Osaka, Japan). The 2,4,6-trinitro-benzensulfonic acid (TNBS, 35,211–44) and Dulbecco's modified Eagle medium (DMEM, 08458–16) were purchased from Nacalai Tesque (Kyoto, Japan). Toluidine Blue O (TBO, 1B-481) was purchased from WALDECK GmbH & Co. KG (Münster, Germany). Ultrapure water was prepared using a Milli-Q water purification system (Direct-Q) from Merck (Darmstadt, Germany). Phosphate-buffered saline (PBS, D5652), Triton X-100 (234,729), and bovine serum albumin (BSA, A3294) were purchased from Sigma-Aldrich (MO, USA). Fetal bovine serum (FBS, 10,270–106), antibiotics (50 U/mL penicillin and 50  $\mu\text{g}/\text{ml}$  streptomycin), and Alexa Fluor® 647 (A21235) were purchased from Thermo Fisher Scientific (MA, USA). Ethanol (14,713–95) and *t*-butanol (028-03386) were purchased from Wako Pure Chemical Industries (Osaka, Japan). NHDFs, human umbilical vein endothelial cells (HUVECs), and endothelial cell growth medium-2

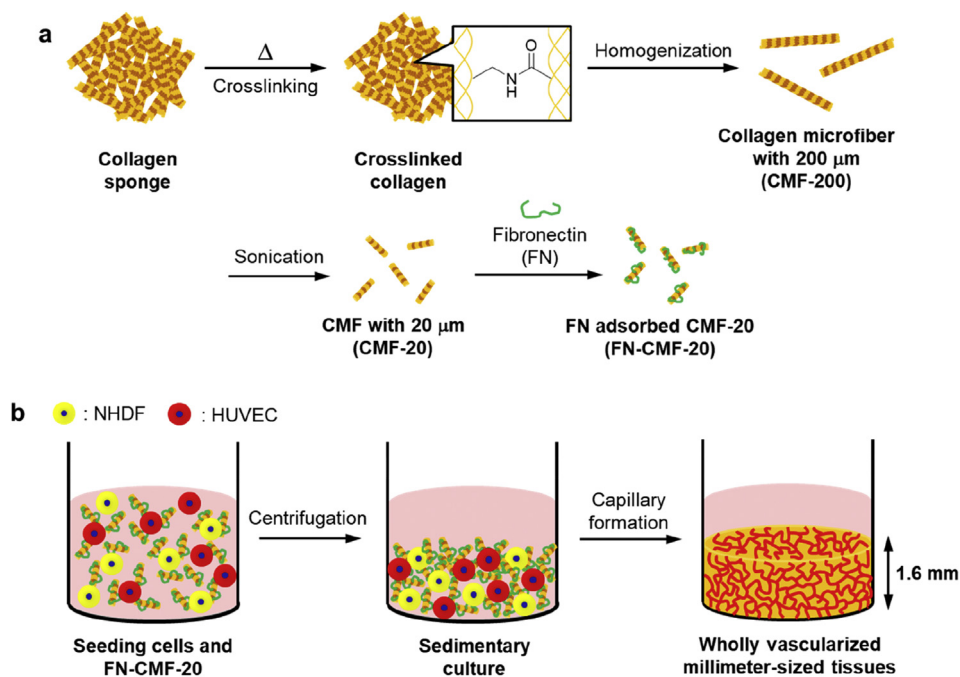


**Fig. 1.** Outline of the present study. (a) Schematic illustration of the fabrication process of collagen microfibers with 200  $\mu\text{m}$  (CMF-200) and 20  $\mu\text{m}$  (CMF-20), respectively. Type I collagen (Col I) was thermally crosslinked before the treatments. Fibronectin-adsorbed CMF-20 (FN-CMF-20) was prepared by adsorption of FN on the surface of CMF-20. (b) Schematic illustration of construction of wholly vascularized millimeter-sized engineered tissues using FN-CMF-20 by sedimentary culture.

(EGM-2, CC-3202) were purchased from LONZA (Basel, Switzerland). Rhodamine fibronectin (Rh-FN, FNR01-A) was purchased from Cytoskeleton (Denver, USA). Fluoresceinamine-labeled chondroitin sulfate A (FITC-CS, FACS-A1), fluoresceinamine-labeled heparan sulfate (FITC-HS, FAHS-P1), and fluoresceinamine-labeled hyaluronan (FITC-HA, FAHA-H1) were purchased from PG Research (Tokyo, Japan). Anti-CD31 antibody (mouse anti-human, NCL-CD31-1A10) was purchased from Leica Biosystems (Wetzlar, Germany).

## 2.2. Thermal crosslinking of type I collagen

To prepare crosslinked Col I, we used a thermal crosslinking method, as previously described [28]. Briefly, the pieces of Col I sponge were put in a vacuum dryer (HD-15H, iLW, Osaka, Japan) and incubated at 100, 150, or 200 °C for 24 h. To evaluate the crosslinking degree of Col I, the primary amine group in the amino acid sequence was measured using TNBS, as previously described [28,29]. Briefly, 0.5 mL of 4% (w/v) NaHCO<sub>3</sub> solution (pH 8.5) and 0.5 mL of freshly prepared 0.5% (w/v) TNBS solution in distilled water were added to 4 mg of the cross-linked Col I. After allowing the reaction to take place for 2 h at 40 °C, 1.5 mL of 6M HCl was added, and the temperature was raised to 60 °C. Solubilization of them was achieved within 90 min 500 μL of the resulting solution was diluted with 10 mL of distilled water, and the absorbance was measured at 345 nm using a UV-vis spectrophotometer (V-670M, JASCO, Tokyo, Japan). The crosslinking degree was calculated by the following equation:

$$\text{Crosslinking degree (\%)} = \{1 - (\text{absorbance}_s / \text{mass}_s) / (\text{absorbance}_n / \text{mass}_n)\} \times 100$$

where the subscripts s and n denote the samples with or without crosslinking, respectively.

The crosslinking degree of their carboxy groups was measured using the TBO method, as previously described [30]. Ten milligrams of the samples were incubated in 30 mL of 0.05% (w/v) TBO solution (pH 10) under stirring at 20 °C for 24 h. The samples were then removed from the solution and rinsed three times in NaOH solution (pH 10) for 10 min under stirring to remove the free TBO. The samples were immersed in 50% acetic acid for 24 h to completely dissolve the adsorbed TBO. After centrifugation of the samples for 5 min at 1000 rpm (5922, Kubota, Tokyo, Japan), the supernatant was diluted with 4 mL of distilled water. The amount of dissolving TBO was detected using the UV-vis spectrophotometer at 620 nm, and the amount of TBO was then calculated using a calibration curve. The Col I sponge with or without crosslinking structure was analyzed by Fourier transform infrared (FT-IR) spectroscopy (Spectrum 100, PerkinElmer, MA, USA). The IR spectrum and the main peaks are shown in Fig. 2c.

## 2.3. Dispersion stability of crosslinked Col I

Ten milligrams of the crosslinked Col I were added in 1 mL of ultrapure water, PBS, or DMEM containing 10% FBS and 1% antibiotics and incubated at 4 °C for 24 h. The remainder in the solutions was collected by centrifugation at 1000 rpm for 5 min and then washing it with ultrapure water for two times. The collected samples were freeze-dried for 3 days (freeze dryer FDU-2200, EYELA, Tokyo, Japan), and then the yields of the samples were estimated.

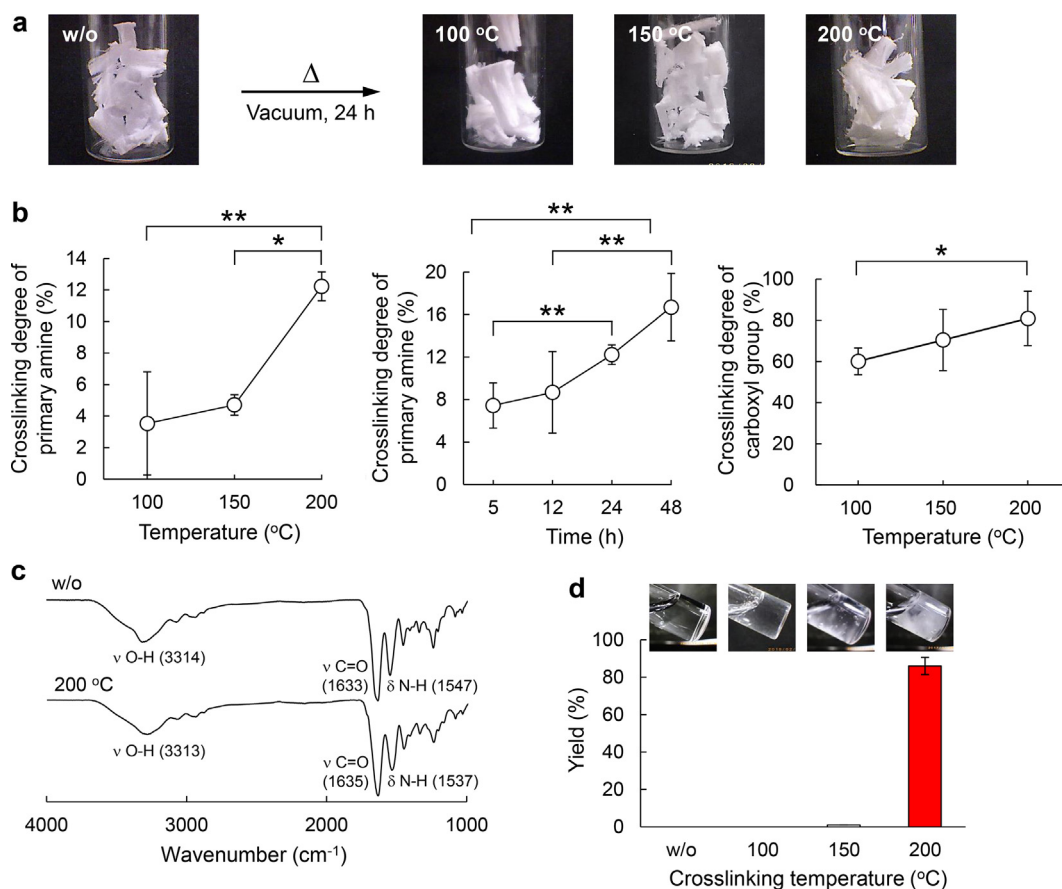


**Fig. 2.** Thermal crosslinking of Col I and their characterization. (a) Photos of Col I and crosslinked Col I at different temperatures under vacuum for 24 h. (b) Effect of crosslinking temperature and time to crosslinking degree calculated by the detection of the remaining primary amine and carboxy groups (n=3). (c) Fourier transform infrared spectra of Col I and crosslinked Col I at 200 °C. (d) Yields and photos of the crosslinked Col I at different crosslinking temperatures after incubation in ultrapure water at 4 °C for 24 h. The remaining Col I was collected by centrifugation at 1000 rpm for 5 min and subsequent freeze-drying for 3 days.

## 2.4. Fabrication of CMFs

To fabricate uncrosslinked CMFs (uCMF-200), the pieces of the freeze-dried sponge of Col I were put in a 15-mL tube and homogenized for 6 min in 5 mL of  $10 \times$  PBS using a homogenizer (Violamo VH-10 homogenizer, S10N-10G diameter of 10 mm and 115 mm length) and then washed once in DMEM without FBS and with 1% antibiotics by centrifugation for 3 min at 10,000 rpm. The length of the obtained CMF was  $210 \pm 90 \mu\text{m}$ , thus it was named as uCMF-200.

For the fabrication of crosslinked CMF (CMF-200), the pieces of the crosslinked Col I at different temperatures were put in a 15 mL tube and homogenized for 6 min in 5 mL of ultrapure water using a homogenizer, washed once in ultrapure water with pipetting, and then collected by centrifugation for 3 min at 10,000 rpm. Ph images of the CMF were observed using a microscope (IX71, Olympus, Tokyo, Japan) and their length was measured using image analysis software ImageJ. The length of the obtained CMF was  $186 \pm 64 \mu\text{m}$ , thus it was named as CMF-200.

To fabricate cell-sized CMF, the CMF-200 dispersion was sonicated by a sonicator (VC50, Sonics and Materials, Newtown, USA) for  $20 \text{ s} \times 100$  times with cooling in ice for 10 s. The dispersion was filtered by a  $42 \mu\text{m}$  nylon mesh (PA-42 $\mu$ , AS ONE, Osaka, Japan) and then freeze-dried for 3 days. Ph images of the CMF were observed using a microscope and their length was measured using ImageJ. The length of the obtained CMF was  $14.8 \pm 8.2 \mu\text{m}$ , thus it was named as CMF-20.

## 2.5. Dispersion property of the CMFs

After centrifugation of the crosslinked and uCMFs dispersion for 3 min at 10,000 rpm, their supernatants were aspirated and the CMFs were freeze-dried for 3 days. They were then added in  $10 \times$  PBS and stirred. Next, the transmittance of 2 mL of 0.5% (w/v) CMF-200 or CMF-20 dispersion in ultrapure water in cuvettes (2-478-03, Kartell, Noviglio, Italy) was measured using the UV-vis spectrophotometer at 600 nm for 60 min. The transmittance of the cuvette was also evaluated as a control of 100%.

## 2.6. Scanning electron microscope observation

Samples were dehydrated in a graded ethanol series in 1 h steps of 50%, 60%, 70%, 80%, 90%, and 100% ethanol, followed by three times in 100% *t*-butanol. The sample was further dried and coated with osmium. Observations were then performed using a field emission scanning electron microscope (JEOL JSM-6701F).

## 2.7. Construction of 3D tissues with blood capillary network

Ten milligrams of uCMF-200, CMF-200, or CMF-20 were mixed with  $1.0 \times 10^6$  cells of NHDF and  $5.0 \times 10^5$  cells of HUVEC in complete DMEM in a total volume of 300  $\mu\text{L}$  inside a 24-well plate transwell (3470, Corning, New York, USA) and 2 mL of DMEM was added outside. The transwells were centrifuged for 20 min at 1100 *g* and 10 °C with low acceleration and deceleration. After 24 h, the transwells were moved to a six-well plate, using an adaptor, and they were cultured in 12 mL of mixed medium (DMEM:EGM-2 = 1:1) inside and outside the transwells with renewal every 3 days. The tissues were cultured for 5 days and subsequently fixed with 4% formaldehyde solution for hematoxylin and eosin (HE) and immunological staining.

## 2.8. Functionalization of CMF-20 by ECM adsorption

One milligram of CMF-20 was added in 1 mL of 0.04 mg/mL Rh-FN, FITC-CS, FITC-HS, or FITC-HA in PBS and stirred for 60 min at 20 rpm using a tube rotor (TR-350, AS ONE, Osaka, Japan). They were then collected by centrifugation at 3500 rpm for 5 min and the supernatant was aspirated. Their adsorption percentage onto CMF-20 was calculated by the difference of fluorescence intensity before and after adsorption of

their supernatant using a spectrofluorometer (FP-8500, JASCO, Tokyo, Japan). The FN-adsorbed CMF-20 (FN-CMF-20) was used for construction of 3D tissues, as stated previously, and then blood capillaries in the tissues were evaluated by the histology and fluorescence images.

## 2.9. Histology and immunohistochemical staining

Samples were fixed in 4% paraformaldehyde solution for 1 h at room temperature and sent to the Applied Medical Research Company for paraffin wax embedding, sections mounting, and HE staining or CD31 and toluidine blue (TB) immunohistological staining. Brightfield images were captured using an FL Evos Auto microscope (AMAFD1000, Thermo Fisher Scientific). The analysis of the staining area percentage and the number of lumen was performed using ImageJ.

## 2.10. Fluorescence imaging of blood capillaries in the 3D tissues

Samples were fixed with 4% paraformaldehyde solution in PBS for 1 h at room temperature. Samples were permeabilized in 0.02% Triton X-100 in PBS overnight at 4 °C and incubated for 1 h at room temperature in 1% BSA in PBS to minimize non-specific staining. Anti-CD31 antibody was added in 1% BSA in PBS and incubated overnight at 4 °C. Finally, the samples were incubated with secondary antibodies Alexa Fluor® 647, at room temperature in the dark for 5 h. The samples were rinsed in PBS and observed using epifluorescence microscopes (Confocal Quantitative Image Cytometer CQ1, Yokogawa, Tokyo, Japan; Confocal Laser Scanning Microscope Fluoview FV3000, Olympus, Tokyo, Japan).

## 2.11. Statistical analysis

All data are expressed as the means  $\pm$  standard deviation (SD), unless otherwise specified. The values represent the means  $\pm$  SD from three independent experiments. Statistical comparisons between groups were analyzed using two-tailed Student's *t*-tests. A *p*-value  $** < 0.05$  and  $* < 0.01$  was considered to be statistically significant.

## 3. Results and discussion

### 3.1. Thermal crosslinking of type I collagen

To obtain thermal crosslinking of type I collagen (Col I), the pieces of Col I sponge were put in a vacuum dryer and incubated at 100, 150, or 200 °C for 24 h (Fig. 2a). As the crosslinked Col I did not change their color or shape after incubation, serious denaturation did not appear to have occurred, which was in agreement with a previous report [27]. To measure the crosslinking degree of the crosslinked Col I, their remaining primary amine and carboxy groups were determined, respectively, by TNBS [28,29] and TBO assays [30] (Fig. S1). The values of crosslinking degree were calculated by comparison with Col I without crosslinking. The crosslinking degree of primary amine groups was increased with increasing incubation temperature and time (Fig. 2b). The crosslinking degrees of primary amine groups at 100, 150, and 200 °C for 24 h were 3.5%, 4.7%, and 12%, whereas the crosslinking degrees of carboxy groups were 34%, 31%, and 63%, respectively. As the amino acids containing primary amine or carboxy groups occupied only 3% and 11% in all of the amino acids of Col I, respectively, 0.36% and 6.9% of the amino acids were crosslinked in total amino acids. FT-IR spectroscopy of Col I with or without crosslinking were undertaken to evaluate the crosslinking bond structure (Fig. 2c). As the IR peaks assigned to the amide I and II groups of the Col I main chain ( $\nu_{\text{C=O}}$ : 1633 and  $\delta_{\text{N-H}}$ : 1547  $\text{cm}^{-1}$ ) were overlapping the newly formed amide groups by the thermal crosslinking, it was difficult to confirm the new amide bond formation by FT-IR analysis.

To understand the crosslinking effect, the dispersion stability of crosslinked Col I sponge was evaluated in ultrapure water, PBS, and DMEM (Figs. 2d and S2). The remaining Col I sponge after incubation in

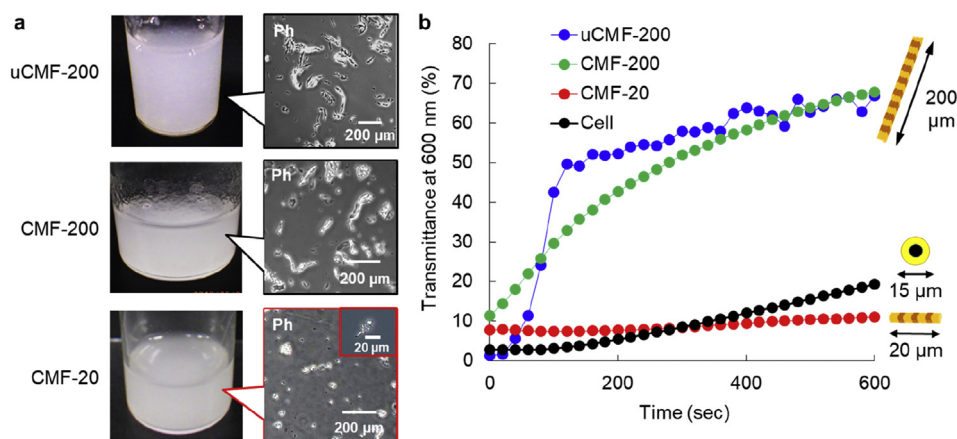


**Fig. 3.** Dispersion stability of CMFs. (a) Photos and phase contrast images (Ph) of uncrosslinked CMF-200 (uCMF-200), CMF-200, and CMF-20 in PBS. (b) The transmittance of 0.5 wt% uCMF-200 and normal human dermal fibroblasts (NHDFs) in PBS and 0.5 wt% CMF-200 and CMF-20 in ultrapure water using a UV–visible spectrophotometer at 600 nm for 600 s. As the uCMF-200 dissolved in water and cells had damage in water, PBS was used for the dispersion study. CMF-200 and CMF-20 were stable in water.

the solutions at 4 °C for 24 h were collected by centrifugation and subsequent freeze-drying. Although the uncrosslinked and crosslinked Col I at 100 and 150 °C were almost dissolved, 86% of the crosslinked Col I at 200 °C was retained, suggesting that 12% and 63% crosslinking of amine and carboxy groups were enough for dispersion stability. Because the piece of a crosslinked collagen sponge was big, it did not disperse well in the solutions. The crosslinked Col I at 200 °C was mainly used for the subsequent experiments.

### 3.2. Fabrication of CMFs

The CMFs without crosslinking were obtained by homogenization, as previously described (Fig. 3a) [26]. As the length of the CMF was  $210 \pm 90 \mu\text{m}$ , as measured using ImageJ software, the uCMF was named as uCMF-200. The uCMF-200 was aggregated and unable to re-disperse in PBS after lyophilization (Fig. S3).

The crosslinked CMF at 200 °C was also obtained by the same method and the length of the crosslinked CMF was  $186 \pm 64 \mu\text{m}$ , thus it was named as CMF-200 (Fig. 3a). The CMF-200 showed high re-dispersion properties in ultrapure water after lyophilization (Fig. S3, Movie S2), probably because of its high stability in water, as shown in Fig. 2d. Although the crosslinked CMFs at 100 and 150 °C were also obtained by homogenization, they were also aggregated and unable to re-disperse in PBS in the same manner as uCMF-200 (Fig. S3) because of a similar instability in water (Fig. 2d). To obtain the cell-sized CMF, additional sonication was performed on CMF-200. As the size of the obtained CMF was  $14.8 \pm 8.2 \mu\text{m}$  (Fig. 3a), it was named as CMF-20. Interestingly, although the CMF-20 showed a uniform sponge shape after lyophilization (Fig. S4), it was also able to immediately re-disperse in ultrapure water (Movie S3). These results suggest that CMF-20 may exhibit lower sedimentation velocity because of its high stability in water and small size.

Supplementary video related to this article can be found at <https://doi.org/10.1016/j.mtbio.2020.100054>

The sedimentation velocity of the CMFs and NHDFs was evaluated by time-dependent transmittance change at 600 nm by a UV–visible spectrophotometer for 600 s just after pipetting (Fig. 3b). For uCMF-200 and NHDFs, PBS was used to avoid dissolving the CMF and damaging the cells. CMF-200 and CMF-20 were dispersed in ultrapure water. Transmittance of both uCMF-200 and CMF-200 solutions increased immediately after 40 s, reaching over 50% after 120 and 280 s, respectively, suggesting high sedimentation velocity. On the other hand, CMF-20 and cells clearly showed almost the same low transmittance continuously until 600 s, indicating almost the same sedimentation velocity probably because of its much smaller size than that of uCMF-200 and CMF-200.

For 3D tissue fabrication, maintaining collagen characteristics of CMF-20 after sonication is important for properties such as cell adhesion. Circular dichroism spectroscopy and electrophoresis are generally used

to confirm the triple helix structure and molecular weight of collagen molecules [27]. However, these methods are not applicable to CMF-20 because of the crosslinking structure. We therefore used anti-Col I antibody immunostaining of lyophilized CMF-20 to ascertain whether the CMF-20 maintained the characteristics of Col I after sonication (Fig. S5). When the CMF-20 does not maintain Col I characteristics, the antibody cannot interact with it. Histological images of the stained CMF-20 clearly show a strong brown color, indicating maintenance of Col I characteristics because of interaction with the antibody.

These results clearly suggest that CMF-20 may solve the problems associated with uCMF-200 during 3D tissue fabrication, which is heterogeneous cell distribution in the obtained tissues.

### 3.3. Effect of CMF size on 3D tissue construction

To evaluate the effect of CMF size on 3D tissue construction, NHDFs and CMFs in DMEM with 10% FBS were mixed and cultured for 5 days by the sedimentary culture method [25,26] (Fig. 4a). The cell viability in the obtained tissues was confirmed by LIVE/DEAD fluorescent staining during culture (Fig. S6). Red-stained cells suggesting dead cells were not observed and green-stained live cells were wholly observed.

Histological images with TB staining were then obtained from the constructed 3D tissues and the cell density was evaluated for quantitative comparison (Fig. 4b and c). Many pores were observed in the obtained 3D tissue using uCMF-200 and CMF-200 and the configuration of cells was not uniform. On the other hand, a dense structure was observed in the obtained 3D tissue using CMF-20 and cell configuration was uniform. Homogeneous cell distribution was clearly observed in the 3D tissues. The cell density of the 3D tissues using CMF-20 was around eight-fold higher than that of CMF-200. We also quantitatively investigated the eosin positive area to determine the ECM area in the 3D tissues from HE staining images because eosin stains ECM (Fig. S7). The eosin positive area of 3D tissues using CMF-200 was 25% of the whole tissue in the histological image, whereas the ECM area of 3D-tissues using CMF-20 was 74%, suggesting a denser structure of the 3D tissues using CMF-20. Although the ECM area of 3D tissues using uCMF-200 was 81%, the same level as CMF-20, the cell density was approximately half that of 3D tissues using CMF-20.

These differences might be the result of the CMF size. The uCMF-200 and CMF-200 had higher sedimentary velocities than the cells (Fig. 3b) because of their much larger relative size. It was therefore difficult for uCMF-200 and CMF-200 to mix with cells uniformly. Conversely, as the CMF-20 was almost the same size as the cells, it was able to mix with cells uniformly and be attracted by the cells, so that a dense structure was obtained. Because of the dense structure of the connective tissues in our body, the CMF-20 would be better suited than the other CMF-200s for tissue engineering.

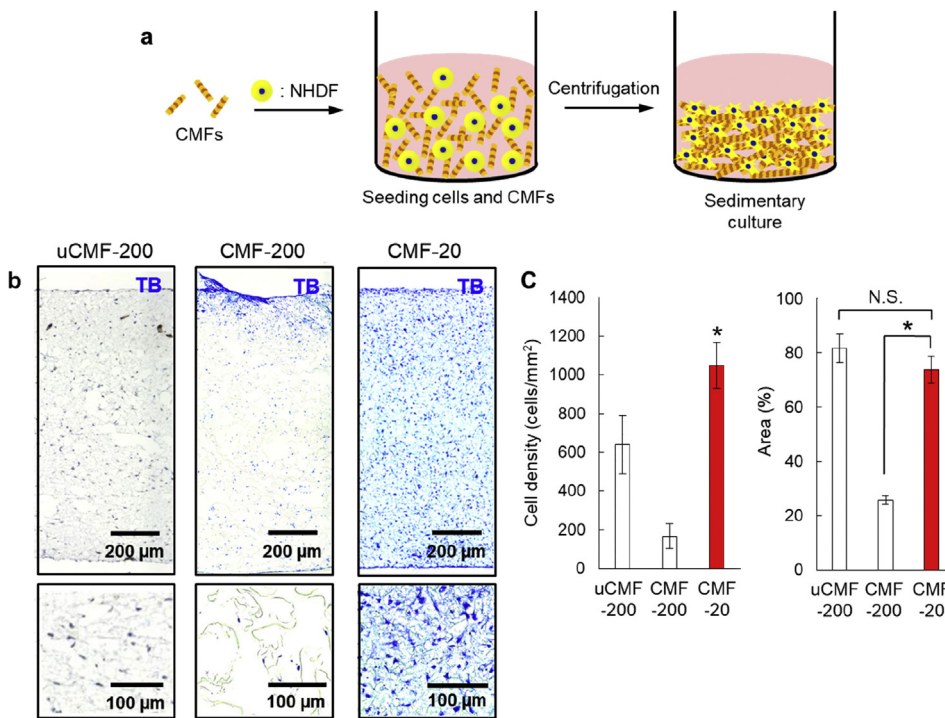


**Fig. 4.** Effect of CMF size on cell density of the fabricated 3D tissues. (a) Schematic illustration of the fabrication of 3D tissues with CMFs by sedimentary culture. (b) Toluidine blue (TB) images of the obtained 3D tissues using uCMF-200, CMF-200, and CMF-20, respectively. The bottoms are magnified images of the uppers. (c) The quantitative comparison of cell density in TB images and ECM area in HE images using CMFs. The asterisks denote statistically significant differences using a two-sample Student's *t*-test ( $*p < 0.01$ ) for each comparison ( $n = 5$ ). The asterisk of CMF-20 for cell density denotes statistically significant difference to both uCMF-200 and CMF-200. (For interpretation of the references to color in this figure legend, the reader is referred to the Web version of this article.)

### 3.4. Functionalization of CMF-20 by ECM adsorption

Although the usability of collagen for *in vitro* construction of 3D tissues has been widely reported with respect to its mechanical strength and cell adhesion, one of the most important functions is a wide variety of interactions with other biomolecules like ECMs including glycosaminoglycans [31]. Living tissues have various ECMs and they are intertwined in a complex fashion, so that various biological functions such as interaction with growth factors [32,33], endothelial cell migration and angiogenesis [34], and cell migration [35] are generated. To obtain these biological functions on the CMF-20, the adsorption of the ECMs such as FN, chondroitin sulfate (CS), heparan sulfate (HS), and hyaluronan (HA) onto the surface of CMF-20 was performed (Fig. 5a).

One milligram of the CMF-20 was added to 1 mL of 0.04 mg/mL Rh-FN, fluorescein isothiocyanate-CS (FITC-CS), FITC-HS, and FITC-HA in PBS and the solutions were stirred at 20 rpm for 60 min. The fluorescence intensity of Rh-FN was slightly observed at the same location of the CMF-20 in a CLSM image after only 5 min of incubation, and markedly increased after 60 min of incubation (Fig. 5b). The location of Rh-FN in fluorescence images overlapped well with Ph image, suggesting that the adsorption of Rh-FN on the surface of CMF-20 was clearly confirmed. Although FITC-CS and FITC-HS were also confirmed by CLSM observation, FITC-HA was rarely observed under the same condition (Figs. 5c and S8).

For a clearer understanding of the phenomena, the adsorption amounts were quantitatively calculated by calibration curves (Figs. 5d

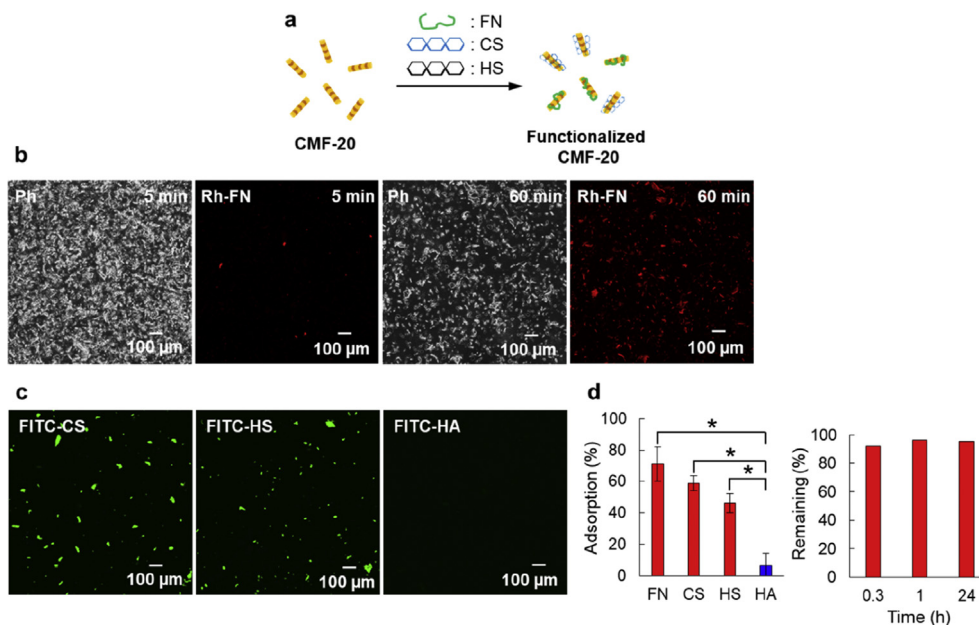


**Fig. 5.** Functionalization of CMF-20 by ECM adsorption. (a) Schematic illustration of the functionalization process of CMF-20 by adsorption of ECMs. (b) Ph and fluorescence images of CMF-20 after mixing with rhodamine-labeled fibronectin (Rh-FN) for 5 and 60 min, respectively. (c) Fluorescent images of CMF-20 after mixing with fluorescein isothiocyanate (FITC)-labeled chondroitin sulfate (CS), heparan sulfate (HS), and hyaluronan (HA) for 60 min. (d) The adsorption percentages of Rh-FN, FITC-CS, FITC-HS, and FITC-HA onto CMF-20 (left) and the remaining percentages of the adsorbed Rh-FN (right) estimated from the remaining fluorescence intensity of supernatants after adsorption. The asterisks denote statistically significant differences using a two-sample Student's *t*-test ( $*p < 0.01$ ) for each comparison ( $n = 3$ ).

**Table 1**  
Adsorption percentage of ECMs on CMF-20.

Sample	Fluorescence intensity <sup>a</sup> (a.u.)	Absorbed amount <sup>b</sup> (mg)	Adsorption percentage <sup>c</sup> (%)
FN	746	0.028	70
CS	897	0.024	60
HS	1032	0.019	48
HA	3378	0.003	8

<sup>a</sup> Fluorescence intensity was measured supernatant of CMF-20 and samples mixture after 60 min with stirring at 20 rpm.

<sup>b</sup> Adsorbed amount of ECMs was calculated by calibration curve (Fig. S8).

<sup>c</sup> Adsorption percentage =  $W_a/0.04$ ,  $W_a$  was the weight of the adsorbed amount, respectively.

and S9). Table 1 summarizes adsorption amounts and percentages of each ECM. The adsorbed percentages of FN, CS, and HS were 71%, 59%, and 46%, respectively, whereas the percentage of HA was only 6%. The adsorption amounts of the ECMs were closely related to the interaction strength such as dissociation constant ( $K_d$ ). For example,  $K_d$  values of between FN, CS, and HS and type I collagen molecule have been reported as  $6.50 \times 10^{-7}$  M,  $1.13 \times 10^{-8}$  M, and  $1.5 \times 10^{-7}$  M, respectively [36–38]. However, because there are no interactions between HA and collagen molecules, HA rarely adsorbed on the surface of CMF-20. The adsorbed Rh-FN was maintained at over 90% even after 1 day of incubation in DMEM with 10% FBS at 37 °C.

These results indicated that functionalization of CMF-20 surfaces by adsorption of ECMs was successful and the adsorbed ECMs were stable during general cell culture conditions. Thus, it is expected that the

functionalized CMF-20 and especially FN-adsorbed CMF-20 (FN-CMF-20) will be useful for stimulating *in vitro* angiogenesis in 3D tissues constructed by sedimentary culture.

### 3.5. Effect of FN-adsorbed CMF-20 on vascularization in 3D tissues

Finally, vascularized millimeter-sized 3D-engineered tissues were fabricated using the FN-CMF-20 by the sedimentary culture method. The CMF-20 or FN-CMF-20 were mixed with NHDF and HUVECs in a culture medium and then seeded into a 24-well plate transwell. After centrifugation, the obtained tissues were cultured for 5 days to fabricate a blood capillary network in the tissues.

Fluorescent immunostaining images with anti-CD31 antibody for HUVEC and anti-vimentin antibody for NHDF were obtained by CLSM observation (Fig. S10). The blood capillary structures in the 3D tissues using both CMF-20 and FN-CMF-20 were clearly observed throughout the whole tissues; however, there were no marked differences between the two CLSM images. Because they were projected images from 3D observations, it was difficult to gain an in-depth understanding of the condition of the blood capillaries. To understand whole vascularization in the millimeter-sized tissues, cross-sectional analysis is especially important. Accordingly, histological images with anti-CD31 antibody immunostaining together with TB staining were compared to both samples.

The thicknesses of both the obtained 3D tissues were approximately 1.6 mm, in which it would be difficult to fabricate a blood capillary network at the center of the tissues (Fig. 6a). The locations of blood capillary lumen structures are denoted by red circles in the histological

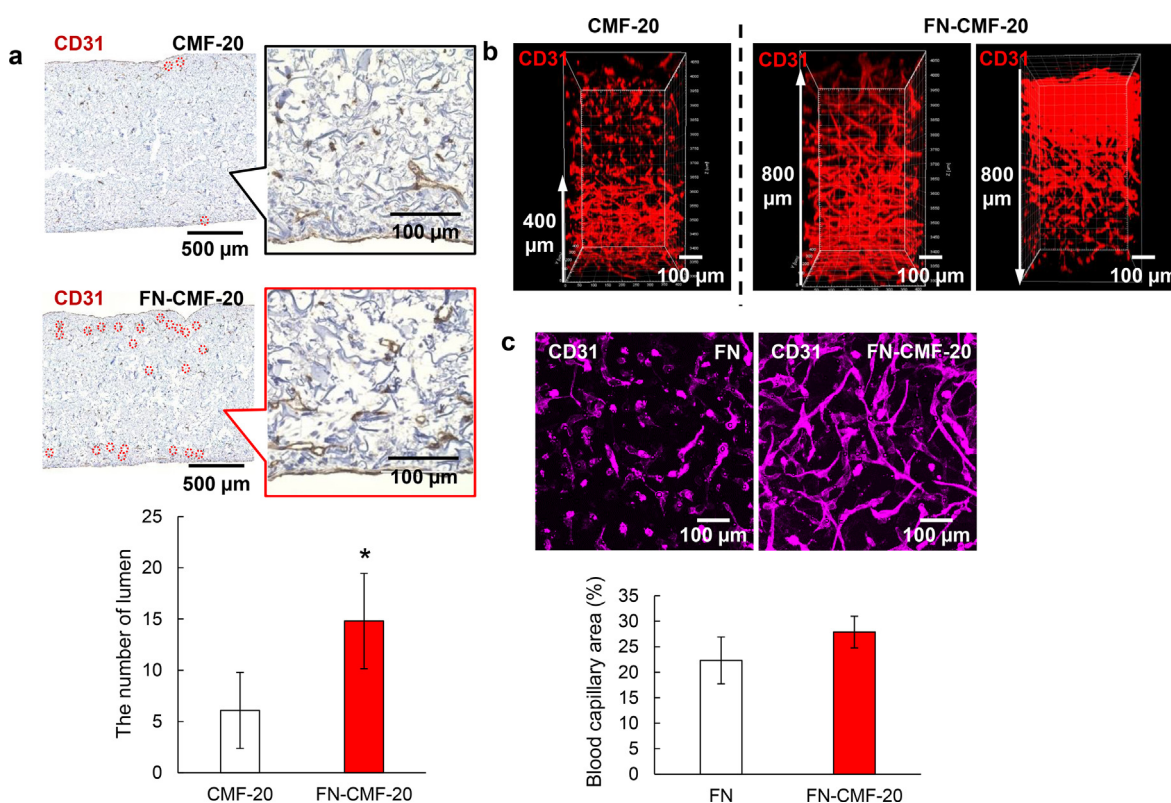


**Fig. 6.** Effect of FN-CMF-20 on vascularization in 3D tissues. (a) Histological immunostaining images with anti-CD31 antibody of the 3D tissues with blood capillaries using CMF-20 and FN-CMF-20, respectively. The inserts show magnified images. Red circles denote the location of blood capillary lumens. The bottom shows the number of lumen at  $0.185 \text{ mm}^2$  in the upper images analyzed by ImageJ software ( $n = 3$ ). (b) 3D-reconstructed CD31 fluorescent immunostaining images of blood capillary networks in 3D tissues using CMF-20 and FN-CMF-20 observed by confocal laser scanning microscopy (CLSM). The FN-CMF-20 samples were observed in 800  $\mu\text{m}$  from bottom to top (left) and top to bottom (right) by CLSM to indicate wholly vascularized structures in 1.6 mm tissues. (c) CD31 fluorescent immunostaining images of blood capillary networks in 3D tissues using CMF-20 with soluble FN and FN-CMF-20 to indicate adsorption effect of FN onto the CMF-20. The bottom shows the percentage of blood capillary area in upper images analyzed by ImageJ software ( $n = 5$ ). (For interpretation of the references to color in this figure legend, the reader is referred to the Web version of this article.)

images. In this study, the definition of the lumen is inner space inside the CD31 positive area [39]. Size of the lumen was almost the same as our previous report, approximately 20  $\mu\text{m}$  [27]. In the tissue with CMF-20, most CD31 positive staining structures were a dot-like shape without lumen and only 17 lumen structures were observed in the one histological image. On the other hand, 55 lumen structures (3.2-fold higher) in the 3D tissue with FN-CMF-20 were clearly observed. Interestingly, the observed lumens in the 3D tissue with FN-CMF-20 were widely spread and some were found near the center. Nuclei of fibroblasts stained with TB but not CD31 antibody were observed in whole tissues using FN-CMF-20, suggesting wide spreading of fibroblast same as the blood capillaries. As it is difficult to evaluate the lumen structures at the precise center inside the 3D tissues, 3D-CLSM observation was performed by fluorescent immunostaining using anti-CD31 antibody from the bottom to a depth of 800  $\mu\text{m}$  (Fig. 6b). The blood capillaries were only observed from the bottom to a depth of 400  $\mu\text{m}$  in the 3D tissue with CMF-20 and isolated dots of HUVEC were observed from 400 to 800  $\mu\text{m}$ . However, well-developed blood capillary networks in the 3D tissue with FN-CMF-20 were observed up to a depth of 800  $\mu\text{m}$ . The whole vascularization was also observed from the top to a depth of 800  $\mu\text{m}$  in the 3D tissues, suggesting whole vascularization in total 1.6-mm thick 3D-engineered tissues. To our knowledge, this is the first report of *in vitro* construction of wholly vascularized millimeter-sized 3D-engineered tissues.

To confirm the effect of the adsorbed FN on CMF-20 on enhancement of angiogenesis in the 3D tissues, FN was dissolved in the culture medium as a soluble factor. Fig. 6c shows CLSM fluorescent immunostaining images of the obtained 3D tissues using CMF-20 together with FN as a soluble factor and the obtained 3D tissues using FN-CMF-20. The CLSM images of the 3D tissues with FN-CMF-20 clearly revealed a denser blood capillary network than that of the 3D tissues with CMF-20 with soluble FN. The quantitative analyses of blood capillary area in both images were 22% for CMF-20 with soluble FN and 28% for FN-CMF-20. We assume that the reason for this phenomenon is a local concentration effect in the 3D tissues. Although the soluble FN was easily diffused in the culture medium, the adsorbed FN on the surface of CMF-20 was stably maintained. Moreover, the adsorbed FN on CMF-20 directly interacted with integrin molecules on the cell membrane at a higher concentration. Accordingly, the FN-CMF-20 exhibited a greater network formation of HUVECs inside 3D tissues even in thickness over 1.6 mm. Such a local concentration effect is applicable to the other ECMs such as CS and HS that have interaction with collagen molecules.

#### 4. Conclusions

In this study, we reported the fabrication of wholly vascularized millimeter-sized engineered tissues using FN-CMF-20. The CMF-200 and CMF-20 were obtained by homogenization and subsequent sonication of the thermally crosslinked collagen. The CMF-20 exhibited a similar sedimentation velocity with cells because of the same size range, thus uniform millimeter-sized tissues with homogeneous cell distribution were fabricated by sedimentary culture. The distribution of the blood capillary network in 1.6-mm-sized engineered tissues was markedly improved by FN-CMF-20. The sedimentary culture using FN-CMF-20 will create new opportunities in tissue engineering for the *in vitro* fabrication of wholly vascularized millimeter-sized engineered tissues. The cell-sized micro-scaffold together with sedimentary culture has enormous potential as a new type of tissue engineering technology for *in vitro* construction of thick 3D tissues such as skin, intestine, gut, bronchial tube, and also diseased models such as an interstitial pneumonia, cirrhosis, myocardial infarction, pancreatic cancer, and breast cancers, etc.

#### Author contributions

M.M. contributed to conceptualization, methodology, writing, supervision, reviewing and editing, project administration, and funding acquisition. Y.N. contributed to methodology, validation, investigation,

and writing the original draft. S.K. contributed to validation and supervision. S.I. contributed to validation and supervision.

#### Declaration of competing interest

The authors declare that they have no known competing financial interests or personal relationships that could have appeared to influence the work reported in this paper.

#### Acknowledgments

All authors thank Nippon Ham Foods Ltd. for their kind donation of collagen. This research was supported by JST-PRESTO (15655131) and JST-MIRAI (18077228), AMED (18be0304207h0002), and a Grant-in-Aid for Scientific Research (B) (17H02099).

#### Appendix A. Supplementary data

Supplementary data to this article can be found online at <https://doi.org/10.1016/j.mtbio.2020.100054>.

#### References

- [1] B.C. Isenberg, J.Y. Wong, Building structure into engineered tissues, *Mater. Today* 9 (2006) 54–60, [https://doi.org/10.1016/S1369-7021\(06\)71743-6](https://doi.org/10.1016/S1369-7021(06)71743-6).
- [2] M. Radisic, L. Yang, J. Boublík, R.J. Cohen, R. Langer, L.E. Freed, G. Vunjak-Novakovic, Medium perfusion enables engineering of compact and contractile cardiac tissue, *Am. J. Physiol. Heart Circ. Physiol.* 286 (2004) 507–516, <https://doi.org/10.1152/ajpheart.00171.2003>.
- [3] E. Lammert, O. Cleaver, D. Melton, Induction of pancreatic differentiation by signals from blood vessels, *Science* 294 (2001) 564–567, <https://doi.org/10.1126/science.1064344>.
- [4] J. Hayashi, *Angiogenesis in vitro*, *Hum. Cell Off. J. Hum. Cell Res. Soc.* 12 (1999) 31–35.
- [5] J.A. Madri, S.K. Williams, Capillary endothelial cell cultures: phenotypic modulation by matrix components, *J. Cell Biol.* 97 (1983) 153–165, <https://doi.org/10.1083/jcb.97.1.153>.
- [6] L.L.Y. Chiu, M. Radisic, Scaffolds with covalently immobilized VEGF and angiopoietin-1 for vascularization of engineered tissues, *Biomaterials* 31 (2010) 226–241, <https://doi.org/10.1016/j.biomaterials.2009.09.039>.
- [7] J.J. Moon, J.E. Saik, R.A. Poché, J.E. Leslie-Barbick, S.H. Lee, A.A. Smith, M.E. Dickinson, J.L. West, Biomimetic hydrogels with pro-angiogenic properties, *Biomaterials* 31 (2010) 3840–3847, <https://doi.org/10.1016/j.biomaterials.2010.01.104>.
- [8] S. Levenberg, J. Rouwkema, M. Macdonald, E.S. Garfein, D.S. Kohane, D.C. Darland, R. Marini, C.A. Van Blitterswijk, R.C. Mulligan, P.A. D'Amore, R. Langer, Engineering vascularized skeletal muscle tissue, *Nat. Biotechnol.* 23 (2005) 879–884, <https://doi.org/10.1038/nbt1109>.
- [9] A. Armulik, G. Genové, C. Betsholtz, Pericytes: developmental, physiological, and pathological perspectives, problems, and promises, *Dev. Cell* 21 (2011) 193–215, <https://doi.org/10.1016/j.devcel.2011.07.001>.
- [10] J.E. Meyer, Brief communications, *Psychiatry* 24 (1961) 357–360, <https://doi.org/10.1521/00332747.1961.11023285> (New York).
- [11] S.J. Grainger, A.J. Putnam, Assessing the permeability of engineered capillary networks in a 3D culture, *PloS One* 6 (2011), <https://doi.org/10.1371/journal.pone.0022086>.
- [12] T. Sasagawa, T. Shimizu, S. Sekiya, Y. Haraguchi, M. Yamato, Y. Sawa, T. Okano, Design of prevascularized three-dimensional cell-dense tissues using a cell sheet stacking manipulation technology, *Biomaterials* 31 (2010) 1646–1654, <https://doi.org/10.1016/j.biomaterials.2009.11.036>.
- [13] N. Asakawa, T. Shimizu, Y. Tsuda, S. Sekiya, T. Sasagawa, M. Yamato, F. Fukai, T. Okano, Pre-vascularization of *in vitro* three-dimensional tissues created by cell sheet engineering, *Biomaterials* 31 (2010) 3903–3909, <https://doi.org/10.1016/j.biomaterials.2010.01.105>.
- [14] Y. Haraguchi, T. Shimizu, T. Sasagawa, H. Sekine, K. Sakaguchi, T. Kikuchi, W. Sekine, S. Sekiya, M. Yamato, M. Umezū, T. Okano, Fabrication of functional three-dimensional tissues by stacking cell sheets *in vitro*, *Nat. Protoc.* 7 (2012) 850–858, <https://doi.org/10.1038/nprot.2012.027>.
- [15] M. Matsusaki, K. Kadowaki, Y. Nakahara, M. Akashi, Fabrication of cellular multilayers with nanometer-sized extracellular matrix films, *Angew. Chem. Int. Ed.* 46 (2007) 4689–4692, <https://doi.org/10.1002/anie.200701089>.
- [16] J.S. Miller, K.R. Stevens, M.T. Yang, B.M. Baker, D.H.T. Nguyen, D.M. Cohen, E. Toro, A.A. Chen, P.A. Galie, X. Yu, R. Chaturvedi, S.N. Bhatia, C.S. Chen, Rapid casting of patterned vascular networks for perfusable engineered three-dimensional tissues, *Nat. Mater.* 11 (2012) 768–774, <https://doi.org/10.1038/nmat3357>.
- [17] Y. Zheng, J. Chen, M. Craven, N.W. Choi, S. Totorica, A. Diaz-Santana, P. Kermani, B. Hempstead, C. Fischbach-Teschl, J.A. López, A.D. Stroock, *In vitro* microvessels for the study of angiogenesis and thrombosis, *Proc. Natl. Acad. Sci. U.S.A.* 109 (2012) 9342–9347, <https://doi.org/10.1073/pnas.1201240109>.

- [18] H. Yoshida, M. Matsusaki, M. Akashi, Multilayered blood capillary analogs in biodegradable hydrogels for in vitro drug permeability assays, *Adv. Funct. Mater.* 23 (2013) 1736–1742, <https://doi.org/10.1002/adfm.201201905>.
- [19] M. Matsusaki, C.P. Case, M. Akashi, Three-dimensional cell culture technique and pathophysiology, *Adv. Drug Deliv. Rev.* 74 (2014) 95–103, <https://doi.org/10.1016/j.addr.2014.01.003>.
- [20] G. Cerino, E. Gaudiello, M.G. Muraro, F. Eckstein, I. Martin, A. Scherberich, A. Marsano, Engineering of an angiogenic niche by perfusion culture of adipose-derived stromal vascular fraction cells, *Sci. Rep.* 7 (2017) 14252, <https://doi.org/10.1038/s41598-017-13882-3>.
- [21] L. Huang, R.P. Apkarian, E.L. Chaikof, High-resolution analysis of engineered type I collagen nanofibers by electron microscopy, *Scanning* 23 (2001) 372–375, <https://doi.org/10.1002/sca.4950230603>.
- [22] Y. Matsumoto, K. Ikeda, Y. Yamaya, K. Yamashita, T. Saito, Y. Hoshino, T. Koga, H. Enari, S. Suto, T. Yotsuyanagi, The usefulness of the collagen and elastin sponge derived from salmon as an Artificial dermis and scaffold for tissue engineering, *Biomed. Res.* 32 (2011) 29–36, <https://doi.org/10.2220/biomedres.32.29>.
- [23] D.A. Young, D.O. Ibrahim, D. Hu, K.L. Christman, Injectable hydrogel scaffold from decellularized human lipoaspirate, *Acta Biomater.* 7 (2011) 1040–1049, <https://doi.org/10.1016/j.actbio.2010.09.035>.
- [24] T. Muthukumar, P. Prabu, K. Ghosh, T.P. Sastry, Fish scale collagen sponge incorporated with *Macrotyloma uniflorum* plant extract as a possible wound/burn dressing material, *Colloids Surf. B Biointerfaces* 113 (2014) 207–212, <https://doi.org/10.1016/j.colsurfb.2013.09.019>.
- [25] D. Su, C.L. Teoh, S.J. Park, J.J. Kim, A. Samanta, R. Bi, U.S. Dinis, M. Olivo, M. Piantino, F. Louis, M. Matsusaki, S.S. Kim, M.A. Bae, Y.T. Chang, Seeing elastin: a near-infrared zwitterionic fluorescent probe for in vivo elastin imaging, *Inside Chem.* 4 (2018) 1128–1138, <https://doi.org/10.1016/j.chempr.2018.02.016>.
- [26] F. Louis, S. Kitano, J.F. Mano, M. Matsusaki, 3D Collagen Microfibers Stimulate the Functionality of Preadipocytes and Maintain the Phenotype of Mature Adipocytes for Long Term Cultures, *Acta Materialia Inc.*, 2019, <https://doi.org/10.1016/j.actbio.2018.11.048>.
- [27] H. Liu, S. Kitano, S. Irie, R. Levato, M. Matsusaki, Collagen microfibers induce blood capillary orientation and open vascular lumen by bioprinting, *Adv. Biosys.* (2020) 2000038, in press.
- [28] N. Nagai, S. Yunoki, T. Suzuki, M. Sakata, K. Tajima, M. Munekata, Application of cross-linked salmon atelocollagen to the scaffold of human periodontal ligament cells, *J. Biosci. Bioeng.* 97 (2004) 389–394, [https://doi.org/10.1016/S1389-1723\(04\)70224-8](https://doi.org/10.1016/S1389-1723(04)70224-8).
- [29] N. Davidenko, C.F. Schuster, D.V. Bax, N. Raynal, R.W. Farnsdale, S.M. Best, R.E. Cameron, Control of crosslinking for tailoring collagen-based scaffolds stability and mechanics, *Acta Biomater.* 25 (2015) 131–142, <https://doi.org/10.1016/j.actbio.2015.07.034>.
- [30] K. Nam, A. Murakoshi, T. Kimura, T. Fujisato, S. Kitamura, A. Kishida, Study on the physical properties of tissue-engineered blood vessels made by chemical cross-linking and polymer-tissue cross-linking, *J. Artif. Organs* 12 (2009) 47–54, <https://doi.org/10.1007/s10047-008-0443-2>.
- [31] R. Parenteau-Bareil, R. Gauvin, F. Berthod, Collagen-based biomaterials for tissue engineering applications, *Materials* 3 (2010) 1863–1887, <https://doi.org/10.3390/ma3031863>.
- [32] T.C. Laurent, U.B. Laurent, J.R.E. Fraser, The structure and function of hyaluronan: an overview, *Immunol. Cell Biol.* 74 (1996) a1–a7, <https://doi.org/10.1038/icb.1996.32>.
- [33] T. Mikami, H. Kitagawa, Biosynthesis and function of chondroitin sulfate, *Biochim. Biophys. Acta Gen. Subj.* 1830 (2013) 4719–4733, <https://doi.org/10.1016/j.bbagen.2013.06.006>.
- [34] R.F. Nicosia, E. Bonanno, M. Smith, Fibronectin promotes the elongation of microvessels during angiogenesis in vitro, *J. Cell. Physiol.* 154 (1993) 654–661, <https://doi.org/10.1002/jcp.1041540325>.
- [35] T. Ohnishi, N. Arita, S. Hiraga, T. Taki, S. Izumoto, Y. Fukushima, T. Hayakawa, Fibronectin-mediated cell migration promotes glioma cell invasion through chemokinetic activity, *Clin. Exp. Metastasis* 15 (1997) 538–546, <https://doi.org/10.1023/A:1018422926361>.
- [36] M.C. Erat, D.A. Slatter, E.D. Lowe, C.J. Millard, R.W. Farnsdale, I.D. Campbell, I. Vakonakis, Identification and structural analysis of type I collagen sites in complex with fibronectin fragments, *Proc. Natl. Acad. Sci. U.S.A.* 106 (2009) 4195–4200, <https://doi.org/10.1073/pnas.0812516106>.
- [37] Y. Tatara, I. Kakizaki, S. Suto, H. Ishioka, M. Negishi, M. Endo, Chondroitin sulfate cluster of epiphysean from salmon nasal cartilage defines binding specificity to collagens, *Glycobiology* 25 (2015) 557–569, <https://doi.org/10.1093/glycob/cwu186>.
- [38] S.M. Sweeney, C.A. Guy, G.B. Fields, J.D. San Antonio, Defining the domains of type I collagen involved in heparin-binding and endothelial tube formation, *Proc. Natl. Acad. Sci. U.S.A.* 95 (1998) 7275–7280, <https://doi.org/10.1073/pnas.95.13.7275>.
- [39] T.L. Stedman, *Illustrated Stedman's Medical Dictionary*, 24<sup>th</sup> Ed., Williams&Wilkins, 1982.